

# **The electric field in northern England and southern Scotland: implications for geomagnetically induced currents**

A.J. McKay<sup>1,2</sup>, K.A. Whaler<sup>1</sup>

<sup>1</sup> *School of Geosciences, Department of Geology and Geophysics, Edinburgh University,  
West Mains Road, Edinburgh, EH9 3JW*

<sup>2</sup> *British Geological Survey, Murchison House, West Mains Road, Edinburgh, EH9 3LA*

Received ; in original form

## **SUMMARY**

Magnetotelluric (MT) data, in the form of MT tensors, are used to estimate directly the size and spatial distribution of the electric field in northern England and southern Scotland with the aim of predicting the flow of geomagnetically induced currents in power networks in the region. MT and Geomagnetic Deep Sounding data from a number of different field campaigns, at a period of 750 s, are employed. The MT data are cast in the form of telluric vectors which allow a joint hypothetical event analysis of both Geomagnetic Deep Sounding and MT data. This analysis reveals qualitatively the pervasive effects of electric field distortion in the region. Two approaches are taken to understand how the spatial structure of the regional electromagnetic field is affected by local distortions, and what the origin of these distortions might be. The dimensionality, and form of electric field distortion, of the MT tensors is investigated using the Weaver et al. (2000) and Bahr (1991) classification schemes, and by examining the misfit of a galvanic distortion model as a function of rotation angle. At sites where the galvanic distortion model is found to be appropriate the regional MT tensors are recovered using tensor decomposition techniques. It is found that recovering the regional MT response reconciles the geometry of induced currents implied by the MT data with that of the Magnetic Variation anomalies. Lilley's (1993) central impedances are used to calculate rotationally invariant effec-

tive telluric responses. In the Southern Uplands the magnitude of the effective telluric response is approximately 0.25-0.5 mV/km.nT, but as the Southern Uplands Fault is approached it rises steadily to 3 mV/km.nT. In the Midland Valley, the effective telluric response is approximately 0.5 mV/km.nT which rises steadily to 2.5 mV/km.nT as the Southern Uplands and Highland Boundary Faults are approached to the south-east and north-west respectively. Therefore, the increase in the magnitude of the effective telluric response correlates with the approach of a major tectonic boundary such as the Southern Uplands Fault. These results show that the induced electric field strength varies considerably throughout the central Scotland region. In addition, the Hypothetical Event Analysis indicates that due to lateral changes in conductivity structure the direction of the electric field deviates significantly from the regional direction implied by the polarisation azimuth of the primary geomagnetic induction. Therefore, any attempts to model the flow of geomagnetically induced currents in the region need to account for the spatial variation of both the magnitude and azimuth of the electric field.

**Key words:** Electromagnetic induction – Electromagnetic modelling – Magnetotellurics – Magnetovariation – Geomagnetically Induced Currents – Distortion analysis.

## 1 INTRODUCTION

During geomagnetic disturbances the geoelectric field at the Earth's surface can cause Geomagnetically Induced Currents (GIC) to flow through conducting networks such as power grids, and gas/oil pipelines. GIC can cause power transformer saturation which can lead to the overload of equipment and malfunction of protective measures installed in the power network (e.g. Molinski 2002). Perhaps the most well-known GIC event is associated with the so-called March 1989 'super-storm' (Bell et al. 1997) during which the Hydro Québec power system collapsed (Boteler et al. 1998). More recently, GIC caused an hour long power cut in southern Sweden (e.g. Pulkkinen et al. 2005).

The geoelectric field is a key quantity (e.g. Viljanen & Pirjola 1994) since the size of GIC is related directly to its magnitude. To investigate the flow of GIC in a power network we need to understand how the geoelectric field responds to a geomagnetic disturbance. The modelling of GIC is often broken down into two parts (e.g. Pirjola 2002). First the geoelectric field is determined,

and then the GIC caused by the geoelectric field are calculated using a suitable model of the power network. In this paper, we concentrate on determining the geoelectric field.

Models of the geoelectric field during particular idealised disturbances are often used to investigate GIC flow. For example, Viljanen et al. (1999) modelled a number of different ionospheric disturbances to investigate the occurrence of large GIC. Their main finding was that large GIC occur during very different geomagnetic events with the main requirement being a large and rapid change of the geomagnetic field. They highlighted the need for accurate models of the Earth's conductivity structure to derive reliable estimates of GIC. However, as was the case with the study of Viljanen et al. (1999), GIC estimates are usually based on one-dimensional Earth conductivity models.

One possibility which has received little attention is the use of measurements of the geoelectric field to investigate GIC. However, the geoelectric field is seldom monitored continuously. Where measurements of the electric field are made, as in a Magnetotelluric (MT) survey, the data are processed to estimate the MT tensor. Estimates of the MT tensor are, in turn, used to infer the conductivity structure of the Earth. However, where we have sufficient data, we can still use the MT tensors to estimate the size and spatial distribution of the geoelectric field directly. The advantage of estimating the electric field using the MT tensors is that such estimates are based on the measurements of the electric field rather than a conductivity model derived from both the electric and magnetic data. However, using the measured MT tensor presents two challenges. Firstly, distortion of MT measurements due to the galvanic response of bodies too small, or shallow, to be involved in induction in the period range of interest is a major problem in the interpretation of MT data (e.g. Groom & Bahr 1992). Galvanic distortion causes the well-known 'static-shift' of the MT apparent resistivity parameter, whose magnitude is shifted up or down by an unknown amount in a frequency independent manner (e.g. Spitzer 2001). Secondly, the spatial distribution of the available long period ( $> 200$  s) MT data is poor. While there is little we can do to improve the spatial coverage, other than making more measurements, tensor decomposition techniques are available to mitigate the problem of galvanic distortion (e.g. Groom & Bailey 1989; Smith 1995).

The northern England and central and southern Scotland (NESS) region is an ideal place to

investigate the utility of MT data in the prediction of GIC in a power network for two reasons. Firstly, the NESS region is covered by the Scottish Power high voltage electricity transmission network, and encompasses the geological terranes of the Midland Valley, Southern Uplands and Concealed Caledonides. Secondly, numerous electromagnetic (EM) induction studies have investigated the crustal conductivity structure of NESS, from Edwards et al. (1971) to Tauber et al. (2003); see Livelybrooks et al. (1993) and Banks et al. (1996) for a fuller list of references. The region has been the subject of intense geophysical (and geological) study because it is thought to be the site of the Iapetus Suture Zone (ISZ). The ISZ corresponds to the join between the crust of North American (Laurentian) affinity (to the north), and European (Avalonian) affinity (to the south); it also marks the site of the closure of the Iapetus Ocean (Livelybrooks et al. 1993).

Two major conductivity anomalies have been identified using the Geomagnetic Deep Sounding (GDS) technique: the Southern Upland and Northumberland Trough anomalies (Banks et al. 1983). The two most recent MT surveys in the region were designed to determine the origin of these two anomalies (Banks et al. 1996), and improve the resolution in the depth range 1-15 km (Tauber et al. 2003). While the main lithological and structural boundaries are aligned NE-SW, associated features may have been disrupted by subsequent faulting, and the complex crustal structure of the ISZ region will affect the spatial distribution of the geoelectric field in a frequency dependent manner. For example, Beamish et al. (2002) employed a simplified 3D model of the UK resistivity distribution to estimate the surface electric field for various amplitudes and orientations of external magnetic field variations. Their model included crustal scale variations in conductivity, which were restricted to terrane boundaries, and the effect of the coastal conductivity contrast. They highlighted the complex redistribution of the electric field amplitude and phase due to both.

Hypothetical event analysis (HEA), where the anomalous internal magnetic fields associated with a 'hypothetical' event due to a uniform horizontal magnetic induction of given magnitude, polarisation and phase, has proved a powerful technique to provide a picture of anomalous currents flowing in response to conductivity structure (e.g. Banks et al. 1983; Egbert & Booker 1993). In this paper, we consider a single variation period of 750 s which is representative of a mode of

induction in a period range which extends from 200 to 2000 s (e.g. Banks & Beamish 1984), where the EM “scattering” response of crustal structures is thought to dominate the observed EM fields. That is, the scale-length of 3D conductivity anomalies is thought to be small in relation to the scale-length of the EM field (e.g. Ritter & Banks 1998; Tauber et al. 2003), and hence the scattered electric field should be in phase with the regional field. Therefore, we should be able to consider induction throughout the NESS region without examining how phase shifts distort the spatial structure of the EM fields. The central period of 750 s is characteristic of the time-scales of variations of auroral sub-storm electrojets (e.g. Rostoker et al. 1997) which are known to be one cause of large GIC (e.g. Viljanen et al. 1999).

The main motivation for this study is to understand better the effect of GIC on technological systems. However, in this paper we concentrate on determining the geoelectric field using the available MT and GDS data. Therefore, the bulk of this paper is concerned with investigating the regional scale EM fields associated with the Southern Uplands and Northumberland Trough conductivity anomalies. We extend the HEA technique by calculating and displaying on the same plot the electric field associated with a unit magnetic induction as well as the anomalous magnetic field. The joint HEA provides a first impression of sites where the electric field is distorted by local structures. In addition, by comparing the joint HEA analysis before and after MT tensor decomposition the success of MT tensor decomposition in removing the local distortion from the MT data can be judged. By considering appropriate rotational invariants of the MT tensor we investigate the dimensionality of the MT data, and estimate how the electric field magnitude varies throughout the region. We argue that the presence of the Southern Uplands and Northumberland Trough conductivity anomalies, and the proximity of the shelf-seas and oceans, will influence GIC in the Scottish Power transmission network by altering the magnitude and direction of the regional electric field.

## 2 DESCRIPTION OF THE DATA

The data are drawn from a number of studies connected with investigating the conductivity structure of northern England and southern Scotland (NESS). The MT data consist of a single period band, centred on 750 s, of all four complex elements of the  $2 \times 2$  MT tensor defined by

$$\mathbf{E} = \mathbf{M} \cdot \mathbf{B} \quad (1)$$

where  $\mathbf{E}$  and  $\mathbf{B}$  (following the notation of Weaver et al. 2000) are the horizontal electric and magnetic induction fields. The MT tensors are expressed in geographic co-ordinates, with units of mV/km.nT (which is equivalent to a velocity). They are therefore telluric response functions (Hobbs 1992). The impedance ( $\mathbf{Z}$ ) of the Earth in Ohms is defined to be,

$$\mathbf{Z} = \mu_0 \begin{bmatrix} M_{xx} & M_{xy} \\ M_{yx} & M_{yy} \end{bmatrix} \quad (2)$$

where  $\mu_0$  is the permeability of free space (Weaver 1994), and  $x$  and  $y$  are the geographic north and east directions. Throughout this paper we work with the telluric response functions, since magnetic measurements are generally quoted with units of nT, and we refer to  $\mathbf{M}$  as the MT tensor (e.g. Weaver et al. 2000). In the form supplied (Banks, 2002, personal communication), error estimates for each tensor element are available only at 15 of the 58 sites. The MT tensor may be expressed in another reference frame ( $x' y'$ ) by rotation i.e.  $\mathbf{M}' = \mathbf{R}_\theta \mathbf{M} \mathbf{R}_\theta^T$ , where  $\mathbf{R}_\theta$  is the matrix for clockwise rotation by an angle  $\theta$  about the positive  $z$ -axis, viz.

$$\mathbf{R}_\theta = \begin{bmatrix} \cos \theta & \sin \theta \\ -\sin \theta & \cos \theta \end{bmatrix} \quad (3)$$

and  $\mathbf{R}_\theta^T$  is the transpose of the rotation matrix.

The GDS data consist of complex-valued single-station GDS transfer functions ( $T_x, T_y$ ) which link the vertical and horizontal geomagnetic induction, viz.

$$B_z = T_x B_x + T_y B_y \quad (4)$$

(e.g. Banks 1973).

## **2.1 Acquisition and Processing**

The MT and GDS data are a sub-set of a much larger database, initially compiled by Livelybrooks et al. (1993) using data acquired by groups at Edinburgh University, the British Geological Survey, and Lancaster University, and subsequently supplemented by a number of studies (Junge 1995; Banks et al. 1996; Tauber et al. 2003). The studies which contributed the majority of the MT data used in this paper are now briefly described; a description of the GDS database may be found in Banks et al. (1993).

Beamish (1986) and Beamish & Smythe (1986) were interested in investigating the deep (30 km) crustal structure of the Northumberland Trough (Figure 1). They employed EDA fluxgate magnetometers for the magnetic field measurements, and non-polarising  $\text{CuSO}_4$  electrodes separated by 100 m for the electric field measurements with a sampling interval of 10 s. The telluric responses were calculated using weighted means of upward and downward biased estimates of each of the tensor elements (e.g. Rokityansky 1982, pp. 193–201).

Banks et al. (1996) attempted to determine the origin of the two main GDS anomalies in NESS thought to be linked to the position of the ISZ. They compiled pre-existing Edinburgh University data and added both new Audio and Long period MT sites, mainly in the Northumberland Trough, in an effort to optimise a MT profile running from the Midland Valley, through the Southern Uplands to the Alston Block (see Figure 1). They employed EDA fluxgate magnetometers, ECA 11 induction coils and lead/lead chloride electrodes to measure the magnetic induction and electric fields. Impedance estimates covering a period range of  $\sim 10^{-2} - 10^3$  s were derived using the robust processing package of Egbert & Booker (1986).

Subsequently, Tauber et al. (2003) improved the resolution of the NESS GDS anomalies in the depth range 1-15 km, and assessed the degree to which the improvement in resolution could be achieved by optimising all aspects from data collection to final modelling. The main MT profile of Tauber et al. (2003) was aligned perpendicular to the strike of the principal Caledonian structures ( $55^\circ$ ); see Figures 1 and 2. Data were acquired with SPAM III systems (Ritter et al. 1998), with both Metronix MFS05 and CM11E induction coils and silver/silver chloride electrodes to measure the magnetic induction and electric fields respectively. The sampling interval was tailored to

the period range of interest. The ‘remote reference’ (e.g. Gamble et al. 1979) facility of SPAM III, in which data from a local base and one or more remote sites may be recorded simultaneously, was employed to establish profiles parallel to the main profile. The side profiles allowed the consistency of structure along the main profile to be assessed, although it was only possible to duplicate part of the main profile (Tauber et al. 2003). Impedance estimates were derived using the robust processing package of Egbert & Booker (1986). The consistency of apparent resistivity and phase estimates were checked using the  $\rho^+$  modelling approach of Parker & Booker (1996) which established an error floor of 3% for the impedance elements (Tauber et al. 2003).

### 3 JOINT ELECTRIC AND MAGNETIC HYPOTHETICAL EVENT ANALYSIS

If we let  $\hat{x}$ ,  $\hat{y}$  be unit vectors in the geographic north and east direction respectively we may define the telluric vectors,  $\mathbf{e}_x$  and  $\mathbf{e}_y$ , as the electric field associated with a unit magnetic induction linearly polarised in a north and east direction respectively, viz.

$$\mathbf{e}_x = M_{xx}\hat{x} + M_{yx}\hat{y} \quad \text{and} \quad \mathbf{e}_y = M_{xy}\hat{x} + M_{yy}\hat{y} \quad (5)$$

(Bahr 1988).

Telluric vectors provide a convenient way to display the MT tensor. Both a real and imaginary telluric vector may be shown graphically. The real part of the telluric vector corresponds to the electric field in phase with the magnetic induction field; the imaginary part is out of phase with the magnetic induction field (Bahr 1988). The telluric vectors may be calculated and displayed in similar way to the Hypothetical Event Analysis (HEA) technique commonly employed in the display and interpretation of GDS anomalies (e.g. Banks et al. 1993; Egbert & Booker 1993).

Figure 3 is a hypothetical event map of the real part of the anomalous horizontal magnetic induction field and telluric vectors associated with a unit magnetic induction (1 nT) linearly polarised in a northerly direction ( $0^\circ$ ) at a period of 750 s. A westerly regional electric field is implied by the polarisation of the magnetic induction field used here. The anomalous horizontal magnetic induction fields were computed from single-station geomagnetic transfer functions using the method described by Banks et al. (1993).

The anomalous horizontal magnetic fields highlight the presence of the two main conductivity anomalies in the region (e.g. Banks et al. 1983; Tauber et al. 2003). The first strikes south-west to north-east, just south of the Southern Uplands fault (SUF); the other strikes east-west and is sandwiched between the Northumberland Trough and Alston Block. These anomalies correlate closely with both major structural features, such as the SUF which divides the Midland Valley terrane from that of the Southern Uplands, and the results of other geophysical techniques (e.g. gravity) (Banks et al. 1996). Both anomalies are thought to originate from a region of high conductivity in the middle-crust (Banks et al. 1996; Tauber et al. 2003). While the anomalies appear continuous, the high-resolution study of Tauber et al. (2003) resolved the south-west end of the SUF conductors into two distinct blocks with edges which mapped to faults expressed in the surface geology.

Some of the difficulties associated with interpretation of the raw MT tensor data are obvious. There are responses which do not appear compatible with neighbouring sites which is manifested as large angular deviations of the telluric vectors from the regional east-west direction, and large amplitude responses. A clear example is provided by the two sites (C1 & C2) at the northern end of Profile C: neither the amplitude nor azimuth of the telluric vectors appear consistent. Similarly, the telluric vectors at two sites (A7 & A9) near the southern end of profile A (Central Scotland) are almost orthogonal, and straddle a similarly sized telluric vector (A8) which is parallel to the strike of the conductivity contrast implied by contours of the anomalous magnetic field. Worth noting however, is the strong but spatially consistent deviation from the regional east-west direction exhibited by the five sites just north of sites A7-A9. The site spacing of profiles A and C are  $\sim 5$  km and  $\sim 2 - 3$  km respectively (Junge 1995; Tauber et al. 2003). At the period considered here (750 s) the inductive scale length is likely to exceed tens of km. Thus, it is reasonable to expect some degree of consistency between sites. These examples indicate that there appear to be both regional and local distortions of the electric field.

In some cases, the magnitude and azimuth of the telluric vectors is inconsistent with the configuration of conductive material implied by the map of the anomalous magnetic induction; Profile B (Northumberland Trough) provides an example. At sites within the 0.1 nT contour (B3-B5) we may have anticipated telluric vectors with a smaller magnitude than the two sites (B1 & B2) which

lie close to the conductivity low implied by the closed 0 nT contour. The opposite is observed: telluric vectors within the region of high conductivity are generally much larger in comparison to sites outwith the region.

#### 4 GEOELECTRIC DIMENSIONALITY OF THE REGION

Rotational invariants of the MT tensor provide some of the most compact parameters embodying the information contained in the MT tensor, and those which characterise the dimensionality of the MT tensor are particularly useful. Weaver et al. (2000) (hereafter WAL) set out criteria for classifying the dimensionality and distortion which are based on seven independent rotational invariants. Similarly, Bahr (1991) proposed a method to assign the MT tensor to one of seven different model classes.

The method of WAL employs rotational invariants of the MT tensor which are zero for particular dimensionality models. The WAL invariants are closely linked to the Mohr circle representation of MT data (e.g. Lilley 1993). The first two invariants,  $I_1$  and  $I_2$ , are based on Lilley's "central impedances" which are defined as

$$I_1 = \frac{1}{2} [(\Re M_{xx} + \Re M_{yy})^2 + (\Re M_{xy} - \Re M_{yx})^2]^{\frac{1}{2}} \quad (6)$$

$$I_2 = \frac{1}{2} [(\Im M_{xx} + \Im M_{yy})^2 + (\Im M_{xy} - \Im M_{yx})^2]^{\frac{1}{2}} \quad (7)$$

where  $\Re$  and  $\Im$  are respectively the real and imaginary parts of the complex tensor element. These two invariants are computed from all the elements of the MT tensor, and when the conductivity structure is 1D the apparent resistivity and phase parameters may be calculated easily. The invariants  $I_3$  and  $I_4$  express the two-dimensionality of the structure, and vanish if the structure is 1D. They arise from the necessary condition of two-dimensionality that there should exist a rotation angle ( $\theta = \theta'$ ; see eqn. 3) for which the diagonal elements of the MT tensor vanish.  $I_5$  and  $I_6$  are related to galvanic distortion of the electric field. They arise from the condition that in regional coordinates the column elements of the MT tensor share the same phase. In other words the telluric vectors each have a single well-defined phase. When  $I_5$  is defined but all higher order invariants are not, then this indicates a pure twist, without shear, of the electric field. If  $I_6$  is defined, the MT

tensor may be decomposed by rotation and real distortion into a regional 2D tensor. In a regional 3D setting there exists no single rotation angle to equalise the phase of each element in the first and second columns of the MT tensor, and  $I_7$  is non-zero. In practice, using real data with noise, the invariants are never zero and a non-zero threshold value, above which the invariants are considered non-zero, must be employed. WAL demonstrated that a threshold of 0.1 was acceptable for realistic numerical data subject to 2% Gaussian noise. Martí et al. (2004) developed error propagation formulae, and found a threshold value of between 0.1-0.15 for data with errors which ranged from 1% at the shortest periods to 30% at the longest periods. We used the threshold originally suggested by WAL of 0.1, and did not explicitly account for data errors.

We proceeded to classify systematically the MT tensors at each site (Figure 1) using the WAL scheme. 27% of the data were difficult to classify confidently. For example, in a number of cases the invariants  $I_6$  and  $I_7$  were contradictory:  $I_6$  would fall well below the threshold required for the interpretation in terms of 3D galvanic distortion of a 2D region, but  $I_7$  would be well-defined suggesting the influence of 3D structure. Alternatively, in some cases the invariants would fall on, or very close to, the threshold. Therefore, for comparison, the dimensionality of the data was investigated using Bahr's distortion classes. Again, some sites proved difficult to classify, but there was not always a one to one correspondence between problematic sites in each of the WAL and Bahr schemes. The results of the analysis are shown in Figure 4.

We consider first the dimensionality as determined using the WAL criteria. Figure 4 shows that almost half of the data are 3D; the other half may mostly be described in terms of some form of galvanic distortion. The galvanic distortion is mostly a 3D distortion of an underlying 2D region. However, there are a number of sites where distortion of the data could be due simply to electrode misalignment, which results in a pure twist of the electric field (Weaver et al. 2000). Fewer data are classified as 3D using the Bahr scheme; for almost 70% of the data a galvanic distortion model may be appropriate. In contrast to the WAL scheme there are 5 sites where the data appear to be 2D. However, these sites were difficult to classify; Bahr's second class, that of a purely local 3D anomaly, may also be appropriate. However, in each of these cases the particular dimensionality class is not well defined.

The dimensionality class obtained using the WAL and Bahr criteria compare well: 40 out of the 58 ( $\sim 69\%$ ) sites fall into a comparable dimensionality class. In undertaking the analysis we chose the minimum value for each of the thresholds suggested by WAL and Bahr. Martí et al. (2004) investigated a range of threshold values to find the most stable dimensionality parameters, and a similar strategy could perhaps be used to optimise agreement between the WAL and Bahr schemes, and find a minimum threshold which provides the most consistent interpretation of the geoelectric dimensionality. However, we chose not to do this as we attempt to fit a galvanic distortion model to the data which takes account of data errors. At almost all of the sites where we found difficulties classifying the dimensionality using the WAL scheme the choice was either between a 3D or 3D distortion of a 2D region. However, at these sites the Bahr skew is invariably less than 0.3, which is below the cut-off threshold suggested by Bahr above which the data should be considered 3D. The Bahr skew performs the same function, and is similar in functional form, to the WAL invariant  $I_7$  but at least for this data-set appears to be less sensitive to noisy data.

Mohr circles were found to be useful to interpret cases where the WAL parameters appear to contradict each other e.g.  $I_6$  is small but  $I_7$  is defined. For example, the Real and Imaginary Mohr circles for the Galloway site C11, which is within the MSZ, are shown in Figure 5. The Mohr circles suggest that the dimensionality of site C11 is likely to be 3D since the centre of both circles is displaced significantly from the  $M_{xy}$  axis (e.g. Lilley 1993). However, the centre of both circles is nearly co-incident, as are the radial arms which join the centre of the circles to the origin. Therefore, the difference of the angles between the Real and Imaginary radial arms and the  $M_{xy}$  axis is small. The sine of the angular difference is precisely what the invariant  $I_6$  measures. Where the WAL parameters lay close to, or on, the threshold values, the Mohr circles were less useful since a choice has to be made regarding the cut-off threshold above which the parameters of the WAL analysis are considered defined.

The results of the WAL, Bahr and Mohr circle analysis highlight the usefulness of considering more than one approach to investigate the dimensionality of MT data. While it may be tempting to re-classify some of the WAL sites, on the basis of, say, the Bahr distortion analysis, we note that

numerical studies have shown that a MT tensor obtained over a 3D conductivity structure can give Bahr skew values below the threshold (Ledo et al. 2002b).

## 5 DECOMPOSITION OF THE MT TENSORS

To form a picture of the spatial variation of the electric fields and currents throughout the region we attempted to separate those distortions of the electric field which are local in nature from the underlying regional response. The joint HEA and dimensionality analysis suggests that most sites are either subject to varying degrees of galvanic distortion or sample 3D structure. Therefore we attempted to fit a galvanic distortion model to the MT tensors taking account of the data errors. It is assumed that magnetic distortion is negligible, and that the measured MT tensor takes the form:

$$\mathbf{M}^m \simeq \mathbf{D} \cdot \mathbf{M}^r \quad (8)$$

where  $\mathbf{M}^m$  is the measured MT tensor,  $\mathbf{D}$  is the telluric distortion matrix which is real and frequency independent, and  $\mathbf{M}^r$  is the regional MT tensor which is assumed to be 2D (e.g. Bahr 1988; Groom & Bailey 1989; Smith 1995).

In the tensor decomposition method of Smith (1995) the regional strike direction is determined by examining the misfit of the distortion model (eq. 8) as a function of tensor rotation angle. In order that simple analytical expressions for the distortion parameters may be employed, independence of the data errors was assumed, which should be approximately true (Smith 1995) when the impedances have been determined using a robust technique (e.g. Egbert & Booker 1986).

### 5.1 Multi-site Analysis

Initially, we assumed that all sites share the same regional 2D structure we aim to recover which is the same assumption made by the sophisticated multi-site analysis of McNeice & Jones (2001). Thus, at each tentative strike angle the distortion model is fitted to the MT data, the misfit computed, and summed over all sites (e.g. Tauber et al. 2003). Assuming an acceptable fit can be established, the strike is the angle at which the misfit is minimised (Smith 1995).

Figure 6 shows the dependence of the total chi-squared misfit ( $\chi^2$ ) on the angle (degrees east

of north) through which the MT tensors were rotated. It can be seen that the misfit changes systematically with rotation, and that a ‘strike’ direction of  $58^\circ$  is suggested. However, the direction has an ambiguity of  $90^\circ$ ; without additional information we cannot say that this corresponds to ‘true’ electrical strike which is defined by the  $E$ -polarisation mode of a 2D conductor. The suggested direction agrees reasonably well with the assumed strike of the major tectonic features of the region of  $52^\circ$  (Tauber et al. 2003), but the fit of the model is poor: the total number of degrees of freedom ( $\nu$ ) is 115 (58 sites each associated with four complex MT tensor elements and 6 fitted parameters, and one strike angle therefore  $\nu = 58 \times (8 - 6) - 1$ ), and for the fit to be deemed acceptable, at the 95% confidence level,  $\log_{10} \chi^2$  should be less than  $\sim 2$ . Given the poor fit of the distortion model when we consider the sites as a single data set, the single-site approach is now examined.

## 5.2 Single-site Analysis

When the strike angle was determined independently at each site, the fit of the distortion model was found to be acceptable at 34 of the 58 sites; see Figure 7. Both the sense of the strike angle is indicated (strike is parallel to the side-bars), and whether the fit of the distortion model is acceptable at the 95% confidence level ( $\chi^2 < 3.8$ ; filled circles). At each of the 34 sites a range of strike angles was found to produce an acceptable fit to the distortion model. The strike angles were well constrained (range of acceptable values limited to within  $\pm 10^\circ$ ) at approximately 75% of these sites. At two sites, all strike angles were found to provide a statistically acceptable fit which may indicate that the data errors have been overestimated. Regardless, the misfit did display a clear minimum consistent with surrounding sites.

For tensor decomposition to be judged successful, the strike direction obtained at each site must be regionally consistent. Indeed, at sites where the fit of the distortion model is acceptable, the determined strike angle is generally consistent with neighbouring sites e.g. the seven sites at the southern end of Profile A (Central Scotland), where the strike angle is  $\sim 60^\circ - 70^\circ$ . However, there are some sites where the strike appears consistent with neighbouring sites, but the fit of the

model is poor e.g. the single site on the east coast near the southern end of Profile A; see also the detailed map of the Profile C (Galloway) sites for more examples.

A change of strike angle is suggested as we move south along Profile B (Northumberland Trough). The strike of the first two sites is  $60^\circ - 65^\circ$  (although the fit of the first site is poor with  $\chi^2 = 29$ ); the strike of southern sites is  $\sim 80^\circ$ . The strike of the southern sites is close to, but less than, the east-west strike suggested by the HEA anomaly map; see Figure 3. For a similar profile, Banks et al. (1996) found a similar dependence of the strike angle using the tensor decomposition method of Groom & Bailey (1989). In addition, the major geological features rotate from  $45^\circ$  in the south western portion of the Southern Uplands to as much as  $90^\circ$  in the vicinity of the Stublick Fault (e.g. Banks et al. 1996). A change in strike angle is also suggested as we move south along Profile C (Galloway). However, the sense of the change is different from that of Profile B. The strike of sites north of the MSZ (the two sites at the northern end of Profile C aside) is  $\sim 85^\circ$ ; the strike of sites south of the MSZ is closer to  $\sim 55^\circ$ . The latter strike direction is closer to both the regional tectonic trends and ‘surface’ geology (Tauber et al. 2003). Thus, the strikes of these sites are taken to be more reliable.

### **5.3 Comparison with dimensionality**

At sites where either the Bahr or WAL invariant analysis suggest the MT tensors are 3D we would expect the fit of the distortion model to be poor. In the Central Scotland profile (A) there are only two sites where the distortion model is found to be inappropriate. For these two sites the WAL and Bahr analysis is contradictory; the WAL analysis suggests that the sites are influenced by 3D structure, but the Bahr analysis suggests that site A3 is subject to weak distortion and that site LL is 2D. Similarly, there are two sites within the Northumberland Trough profile (B) where the fit of the distortion model is found to be poor, and the WAL and Bahr analysis is contradictory. At sites in the Galloway survey where the fit of the distortion model is poor both the WAL and Bahr analysis suggests that the poor fit is due to the influence of 3D structure. In these cases the Bahr analysis performs slightly better than the WAL analysis as it seems to reflect better the spatial

variation of the model fit, particularly at the southern end of the main profile where the influence of 3D structure and galvanic distortion alternates as we move along the profile.

## 6 THE REGIONAL RESPONSE

At sites where the fit of the distortion model was found to be acceptable the regional responses ( $M^r$ ; eq. 8) were recovered. The strike angle found at each site was used to define the regional coordinate system of the MT tensor. After recovery of the regional response, the regional MT tensors were rotated back to geographic coordinates to display the results in the form of telluric vectors. The real  $e_x$  telluric vectors after the decomposition procedure are shown in Figure 8. In comparison with Figure 3, the decomposition has generated considerable inter-site consistency in telluric vector azimuth: the large angular deviations of the telluric vector from the regional azimuth noted previously have vanished. The telluric vectors are now generally consistent with those expected for the polarisation azimuth of the primary magnetic induction, and the configuration of conductive material suggested by the spatial pattern of the anomalous horizontal magnetic induction.

We would like to estimate an ‘average’ electric field associated with a unit geomagnetic disturbance. However, an inherent limitation of the tensor decomposition schemes is that without additional information the extent to which the regional electric field is ‘amplified’ via galvanic distortion is indeterminate. There are a number of strategies for overcoming this. For example, the static shift parameter, which describes the effect of this amplification of the electric field on the apparent resistivity, can be solved for using a joint inversion of MT and GDS data (e.g. Livelybrooks et al. 1993). In the special case where the spatial derivative of the horizontal magnetic field may be neglected, Ledo et al. (2002a) show how GDS functions may be used to remove the static-shift and partially recover the regional  $E$ -polarisation response. Here we use a simple approach since we need only remove those sites which distort significantly our estimate of an average regional electric field.

For each of the profiles shown in Figure 1 Lilley’s central impedances were used to calculate a rotationally invariant measure of the telluric response which we call the central telluric response. Error estimates were calculated using the formulae given by Martí et al. (2004) which were derived

using classical error propagation. The central telluric response is shown for each of the three profiles (Figure 1) in Figure 9. Each profile strikes approximately north west to south east. Distance, in km, is measured relative to the first site at the northern end of each profile; the position of major geological features are marked.

The main features traversed by Profile A are the Highland Boundary Fault (HBF) in the north west and the Southern Uplands Fault (SUF) in the south east (e.g. McKerrow 1986). Immediately south of the SUF are negative Bouguer gravity anomalies thought to be produced by granite batholiths (Lagios & Hipkin 1982; Banks et al. 1996). The main feature traversed by Profile B is the Stublick Fault (SF) which marks the boundary between the Northumberland Trough and Alston Block. Profile C encompasses the tectonic terrane of the Southern Uplands and the Moniaive Shear Zone (MSZ), a ductile shear zone approximately 5 km wide. It also crosses numerous tract bounding faults (Tauber et al. 2003); see Figure 2.

Some spatial consistency of the effective telluric response is observed within profiles A and C, and the similar shape of profiles A and C is interesting. Profile A is bounded by the major tectonic terranes of the Central Highlands and Southern Uplands to the north and south respectively. Profile C lies entirely within the tectonic terrane of the Southern Uplands: the northern end of profile C is  $\sim 5$  km from the SUF (Tauber et al. 2003). Profile B appears less consistent, but the strike is less well-defined and the station spacing is larger than the other two profiles.

Two minima in the Profile C telluric response occur on either side of the MSZ. These minima are coincident with zones of high electrical conductivity ( $\sim 4 - 12$  km depth) identified in Tauber et al.'s (2003) *B*-polarisation phase pseudo section, and best fitting 2D model derived from inverting the *B*-polarisation mode MT data; the relative high within the MSZ coincides with a zone of lower conductivity over the same depth range, the origin of which is uncertain (see Tauber et al. 2003, for further details). Tauber et al. (2003) also commented on the influence of major structural features beyond the ends of the profile: the results of the inversion show a deepening of the conductive layer to the north, under the Midland valley, and a conductive zone (depth  $\geq 12$  km) beneath the southern end. However, given the poor control provided by single sites situated at each end of the profile, and the need to satisfy the 2D model boundary conditions, they judged the features to

be insufficiently robust to warrant further discussion. At the northern end of profile C the real part of the central telluric response rises smoothly (over a distance of 10 km) from  $\sim 0.25$  mV/km.nT to  $\sim 3$  mV/km.nT, as the SUF is approached. Similarly, at the southern end of profile A, the real part of the central telluric response rises smoothly from  $\sim 0.5$  mV/km.nT to  $\sim 2.25$  mV/km.nT over a similar distance as the SUF is approached. The magnitude and spatial variation of the real and imaginary central telluric response at sites near the south east end of profile A is similar to that of sites at the north western end of profile C. If we displaced profile C approximately 100 km to the north east, along the strike of the SUF, then the ends of profiles A and C would match rather well across their common boundary of the SUF. Thus the steep rise in the modulus of the telluric response at each end of the profile may reflect the proximity to the major tectonic terrane boundary.

The spatial variation of the central telluric response is consistent with the Southern Uplands being generally more conductive than the Midland Valley to its north. We can use the magnitude of the telluric response to estimate the size of the electric fields. At distances greater than  $\sim 10$  km from the major tectonic boundaries, the magnitude of the effective telluric response of sites within the Midland Valley is approximately double that of sites within the tectonic terrane of the Southern Uplands.

## **7 DISCUSSION & CONCLUSIONS**

The joint Hypothetical Event Analysis highlighted the disparity between the spatial distribution of induced currents implied by the GDS and MT data. To obtain a regionally consistent picture of the geometry of induced electric fields we used the tensor decomposition method of Smith (1995). The tensor decomposition was justified because the dimensionality and distortion analysis indicated that the data from most sites are affected by varying degrees of galvanic distortion, while some are likely to be affected by 3D structure. The majority of sites for which 3D structure is implied are located south of the Moniaive Shear Zone (Profile C, Galloway) which is consistent with the findings of Tauber et al. (2003) where out-of-quadrant phases and a change in the azimuth of induction arrows were both observed. A multi- and single-site approach to the determination of

electrical strike was undertaken. While the multi-site analysis suggested a regional strike direction of  $58^\circ$ , which is in good agreement with the trends of the major regional structure, the fit of the distortion model was poor, and was rejected at the 95% confidence level. Using a single-site approach, the fit of the distortion model was acceptable at the 95% confidence level for 34 of the 58 sites considered. The strike directions we determined were found to be generally consistent with the electromagnetic strike implied by the GDS anomalies i.e. approximately  $60^\circ$  in the vicinity of the Southern Uplands, and about  $80^\circ - 90^\circ$  in the vicinity of the Northumberland Trough. Recovering the regional MT response from the decomposed tensors reconciled the spatial structure of the electromagnetic fields implied by the GDS and MT data.

We found it useful to consider more than one approach to investigate the dimensionality of the MT data. It was not a goal of this study to compare the WAL and Bahr analysis. Generally applicable conclusions cannot be drawn as we chose the minimum thresholds without explicitly considering data noise. However, the MT data we used are a good test of the various techniques we employed since they span a period of time in which the processing of MT data has advanced considerably. Weaver et al. (2000) highlight that the invariant  $I_7$  is sensitive to noise while each of the six other invariants (and the supplementary invariant  $Q$ ) are robust. We note that for many of the sites where the seventh WAL invariant fell on or very close to the cut-off threshold, and we have assumed a 3D distortion of a 2D region, the Bahr skew was generally small and a statistically acceptable fit of the decomposition could be established. Martí et al. (2005) illustrated that the WAL  $Q$  parameter may improve Bahr's analysis; we think that it may be useful to supplement the WAL analysis with Bahr's skew. However, this study provides evidence based on measured data which supplements the numerical modelling results of Ledo et al. (2002b) which show that a small Bahr skew is a necessary, but not sufficient condition, for the dimensionality of the MT tensor to be less than 3D. For example, similar Mohr circles are obtained to those shown in Figure 5 for two Galloway sites 52 and 53 (see Figure 2). These Mohr circles and the WAL analysis suggest a 3D dimensionality, and the decomposition model can be rejected at the 95% confidence level, but the Bahr skew is small.

Our main motivation for calculating an effective telluric response using Lilley's central impedances

was that they are compact, and are calculated using all of the elements of the MT tensor. In addition, invariant responses have in some special cases been shown to provide an element of distortion correction (e.g. Berdichevsky et al. 1989). Some have argued (e.g. Groom & Bailey 1989), and others demonstrated by modelling (e.g. Jiracek 1990, and references therein), that the effective telluric response may still only represent the regional telluric response up to an unknown static shift factor. If we wished to use the MT data to extract a conductivity model of the Earth, then this unknown scaling factor would be a problem. Here however, we need only an estimate of the total electric field, and because spatially consistent sets of the effective telluric response were obtained for profiles A (Central Scotland) and C (Galloway) we can use these as representative of the magnitude of the total electric field of each of the areas traversed. We found that within the Galloway profile, low (0.25 mV/km.nT) effective telluric responses correlated closely with two zones of high electrical conductivity in the depth range 4-12 km which are thought to be the source of the SUF anomaly (Tauber et al. 2003); within the Midland Valley the effective telluric response is 0.5 mV/km.nT. The effective telluric responses are relatively smooth along the Midland Valley and Southern Uplands profiles. These profiles suggest that the regional electric fields in the Midland Valley are approximately double those in the Southern Uplands. However, some care is required closer to the boundaries of these two regions: the similarity between the central telluric response of sites at the south eastern and north western end of profiles A and C respectively suggests that the effective telluric response may be larger ( $\sim 1 - 3$  mV/km.nT) about 10 km either side of the SUF.

To turn estimates of the effective telluric response into useful estimates of the geoelectric field we need to know the typical amplitude of magnetic variations at a period of 750 s. Pulkkinen et al. (2003) considered in detail a large geomagnetic storm which occurred in April 2000 and caused GIC in both Finland and the United Kingdom. Some of the largest GIC during this storm were observed during an intense Westward Electrojet. Inspection of the magnetograms from Eskdalemuir geomagnetic observatory suggests that the north component of the geomagnetic field varied by approximately 800 nT over a period of about 10 minutes (McKay 2004). Therefore, electric field amplitudes in the Midland Valley and Southern Uplands were likely to be around 0.4 V/km and 0.2 V/km respectively; within 10 km either side of a major boundary such as the SUF then

the electric field amplitude could reach 2.4 V/ km. The magnitude of the electric field at any given period is one factor which will control the amplitude of GIC: the spatial geometry of the fields will also influence the distribution of GIC. Indeed, the hypothetical event analysis shows that the direction of the induced geoelectric field deviates from the regional east-west direction when the geomagnetic induction is polarised north. In particular, electric field vectors in the Southern Uplands region point along the axis of the Southern Uplands anomaly which strikes north-east to south-west.

One of the aims of this study was to develop an understanding of the regional EM fields which justified the approach we took to reconcile the MT and GDS data. However, it is not clear how local distortion of the electric field will affect GIC. The voltage between two ends of a conductor such as a power line is equal to the line integral of the electric field along the path of the conductor (e.g. Gomez-Trevino 1992; Viljanen & Pirjola 1994). Therefore, in GIC studies, it is usually assumed that variations of the electric field which occur on a small spatial scale are unimportant because integration smooths the electric field, and the conductors in a power network are long (e.g. Viljanen & Pirjola 1994). However, this smoothing operation requires that the small-scale electric field can be characterised as random noise (e.g. Viljanen & Pirjola 1994). It is not self-evident that the spatial variability of the electric field in the NESS region may be described as random. In addition, the extent to which the smoothing property is satisfied will be guided by both the spatial-scales of the power network (i.e. the typical length of connections in the network) and the electric field. Both require further study before firm conclusions can be drawn.

The coast effect, where the on-shore electric field magnitude is enhanced because of the mismatch in the conductivities of the ocean and land is considered important for GIC (e.g. Beamish et al. 2002). For example, power generation plant is often located close to the coast to simplify cooling arrangements (e.g. Gilbert 2005). The southern sites of Profile A are interesting: these sites presumably sense the EM fields associated with both the SUF anomaly and the coastal conductivity contrast. The amplitude of the three most easterly telluric vectors is enhanced in comparison to the inland sites (A4-A9) which suggests that the coastal effect contributes to the response; see Figures 1 and 8. The azimuth of the telluric vectors is less revealing because it is consistent with

both the strike of the SUF, and the strike of the coastline. Both the coastal conductivity contrast and the SUF will impart the same sense of rotation on the regional current flow e.g. a regional east west current will be deflected to the south west.

This particular study provides a snapshot of the electromagnetic fields at a period of 750 s for a given polarisation azimuth and phase of the primary magnetic induction. In future, we intend to extend the period range to both longer and shorter periods. The largest GIC are often associated with rapid variations of the geomagnetic field (e.g. Viljanen 1997), but to gain a full understanding of the risk posed to power networks we also need to investigate longer period variations, such as substorm expansion, which can last for about 30 minutes and affect a wide geographic area (e.g. Pulkkinen et al. 2003). Increasing the period range is probably best done using a combination of the data-based investigation as was employed here in tandem with a numerical model (e.g. Thomson et al. 2005). Indeed if we are to be able to calculate GIC then we would need to ‘interpolate’ the sparse MT measurements in some fashion. It is worth investigating whether the HEA map can be used for the purpose of interpolation. Throughout this paper we have made the implicit assumption that the primary magnetic induction is uniform across our study area. While this assumption is most likely a fair approximation when the field is quiescent it is unlikely to be true during a major geomagnetic disturbance. Nevertheless, we still can gain an understanding of the dimensionality of models we need to employ to understand and model the electric field response.

## **ACKNOWLEDGMENTS**

The research described in this paper was supported by Engineering and Physical Sciences Research Council award number 99316793. Dr Alan Thomson is thanked for his useful comments and suggestions regarding this work. The comments and suggestions of the Editor and two anonymous referees improved this paper, and their contribution is gratefully acknowledged. In particular, one referee suggested inclusion of the Mohr circle analysis. This paper is published with the permission of the Executive Director, British Geological Survey (NERC).

## REFERENCES

- Bahr, K., 1988. Interpretation of the Magnetotelluric impedance tensor: regional induction and local telluric distortion, *J. Geophys.*, **62**, 119–127.
- Bahr, K., 1991. Geological noise in magnetotelluric data: a classification of distortion types, *Phys. Earth planet. Inter.*, **66**, 24–38.
- Banks, R.J., 1973. Data processing and interpretation in geomagnetic deep sounding, *Phys. Earth planet. Inter.*, **7**, 339–348.
- Banks, R.J., Beamish, D. and Geake, M.J., 1983. Magnetic variation anomalies in northern England and southern Scotland, *Nature*, **303**, 516–518.
- Banks, R.J. and Beamish, D., 1984. Local and regional induction in the British Isles, *Geophys. J. R. astr. Soc.*, **79**, 539–553.
- Banks, R.J., Irving, A.A.K. and Livelybrooks, D.W., 1993. The simulation of magnetic variation anomalies using single-station data, *Phys. Earth planet. Inter.*, **81**, 85–98.
- Banks, R., Livelybrooks, D., and Longstaff, R., 1996. Causes of high crustal conductivity beneath the Iapetus suture zone in Great Britain, *Geophys. J. Int.*, **124**, 433–455.
- Beamish, D., 1986. Deep crustal geoelectrical structure beneath the Northumberland Basin, *Geophys. J. R. astr. Soc.*, **84**, 619–640.
- Beamish, D., Clark, T.D.G., Clarke, E. and Thomson, A.W.P., 2002. Geomagnetically induced currents in the UK: geomagnetic variations and surface electric fields, *J. Atmos. Sol. Terr. Phys.*, **64**, 1779–1792.
- Beamish, D. and Smythe, D., 1986. Geophysical images of the deep crust: the Iapetus suture, *J. Geol. Soc. London*, **143**, 489–497.
- Bell, J.T., Gussenhoven, M.S. and Mullen, E.G., 1997. Super storms, *J. geophys. Res.*, **102**, 14,189–14,198.
- Berdichevsky, M.N., Vanyan, L.L. and Dmitriev, V.I., 1989. Methods used in the U.S.S.R. to reduce near-surface inhomogeneity effects on deep magnetotelluric sounding, *Phys. Earth planet. Inter.*, **53**, 194–206.
- Boteler, D.H., Pirjola, R.J. and Nevanlinna, H., 1998. The effects of geomagnetic disturbances on electrical systems at the Earth's surface, *Adv. Space Res.*, **22**, 17–27.
- Edwards, R.N., Law, L.K. and White, A., 1971. Geomagnetic variations in the British Isles and their relation to electrical currents in the oceans and shallow seas, *Phil. Trans. R. Soc. Lond.*, **A270**, 289–323.
- Egbert, G. and Booker, J., 1986. Robust estimation of geomagnetic transfer functions, *Geophys. J. R. astr. Soc.*, **87**, 173–194.
- Egbert, G.D. and Booker, J.R., 1993. Imaging crustal structure in south-western Washington with small magnetometer arrays, *J. geophys. Res.*, **98**, 15,967–15,985.
- Gamble, T., Goubau, W., and Clarke, J., 1979. Magnetotellurics with a remote magnetic reference, *Geophysics*, **44**, 53–68.
- Gilbert, J.L., 2005. Modeling the effect of the ocean-land interface on induced electric fields during geo-

- magnetic storms, *Space Weather*, **3**, doi:10.1029/2004SW000120.
- Gomez-Trevino, E., 1987. Should the electric line be straight in magnetotelluric surveys? *Geophys. Prosp.* **35**, 920–923.
- Groom, R.W. and Bahr, K., 1992. Corrections for near surface effects: decomposition of the magnetotelluric impedance tensor and scaling corrections for regional resistivities: a tutorial, *Surv. Geophys.* **13**, 341–379.
- Groom, R.W. and Bailey, R.C., 1989. Decomposition of magnetotelluric impedance tensors in the presence of local three dimensional galvanic distortion, *J. geophys. Res.*, **94**, 1915–1925.
- Hobbs, B., 1992. Terminology and symbols for use in studies of electromagnetic induction in the Earth, *Surv. Geophys.*, **13**, 489–515.
- Jiracek, J., 1990. Near surface and topographic distortions in electromagnetic induction, *Surv. Geophys.*, **11**, 163–203.
- Junge, A., 1995. Magnetotellurics in the long period range, Final Report, Tech. rep., EEC Human Capital and Mobility contract No. ERBCHBICT 93 0610.
- Lagios, E. and Hipkin, R., 1982. A geophysical approach to the granite batholith under the Eastern Southern Uplands, *Pure appl. Geophys.*, **129**, 375–388.
- Ledo, J., Gabás, A. and Marcuello, A., 2002a. Static shift levelling using geomagnetic transfer functions, *Earth Planets Space*, **54**, 493–498.
- Ledo, J., Queralt, P., Martí, A. and Jones, A.G., 2002b. Two-dimensional interpretation of three-dimensional magnetotelluric data: an example of limitations and resolution, *Geophys. J. Int.*, **150**, 127–139.
- Lilley, F.E.M., 1993. Magnetotelluric analysis using Mohr circles, *Geophysics*, **58**, 1498–1507.
- Livelybrooks, D., Banks, R., Parr, R., and Hutton, V., 1993. Inversion of electromagnetic induction data for the Iapetus Suture Zone in the UK, *Phys. Earth planet. Inter.*, **81**, 67–84.
- Martí, A., Queralt, P. and Roca, E., 2004. Geoelectric dimensionality in complex geological areas: application to the Spanish Betic Chain, *Geophys. J. Int.*, **157**, 961–974.
- Martí, A., Queralt, P., Jones, A.G. and Ledo, J., 2005. Improving Bahr's invariant parameters using the WAL approach, *Geophys. J. Int.*, **163**, 38–41.
- McKerrow, W., 1986, The tectonic setting of the Southern Uplands, in *Synthesis of the Caledonian rocks of Britain*, Kluwer Academic.
- McKay, A.J., 2004, Geoelectric fields and geomagnetically induced currents in the United Kingdom, PhD Thesis, University of Edinburgh (<http://www.era.lib.ed.ac.uk/1842/639>), 237 pp.
- McNeice, G.W. and Jones, A.G., 2001. Multi-site, multi-frequency tensor decomposition of magnetotelluric data *Geophysics*, **66**, 158–173.
- Molinski, T.S., 2002. Why utilities respect geomagnetically induced currents, *J. Atmos. Sol. Terr. Phys.*

**64**, 1765–1778.

- Parker, R. and Booker, J., 1996. Optimal one-dimensional inversion and bounding of magnetotelluric apparent resistivity and phase measurements, *Phys. Earth planet. Inter.*, **98**, 269–282.
- Pirjola, R., 2002. Review on the calculation of surface electric and magnetic fields and of geomagnetically induced currents in ground-based technological systems, *Surv. Geophys.*, **23**, 71–90.
- Pulkkinen, A., Thomson, A., Clarke, E. and McKay, A., 2003. April 2000 storm: ionospheric drivers of large geomagnetically induced currents, *Ann. Geophys.*, **21**, 709–717.
- Pulkkinen, A., Lindahl, S., Viljanen, A. and Pirjola, R., 2005. Geomagnetic storm of 29–31 October 2003: geomagnetically induced currents and their relation to problems in the Swedish high-voltage power transmission system, *Space Weather*, **3**, doi:10.1029/2004SW00123.
- Ritter, P. and Banks, R.J., 1998. Separation of local and regional information in distorted GDS response functions by hypothetical event analysis, *Geophys. J. Int.*, **135**, 923–942.
- Ritter, O., Junge, A., and Dawes, G., 1998. New equipment and processing for magnetotelluric remote reference observations, *Geophys. J. Int.*, **132**, 535–548.
- Rokityansky, I., 1982. *Geoelectric Investigation of the Earth's Crust and Mantle*, Springer–Verlag.
- Rostoker, G., Friedrich, E., and Dobbs, M., 1997. Physics of Magnetic Storms, in *Magnetic Storms*, American Geophysical Union, Geophysical Monograph 98, 149–160.
- Smith, J.T., 1995. Understanding telluric distortion matrices, *Geophys. J. Int.*, **122**, 219–226.
- Spitzer, K., 2001. Magnetotelluric static shift and direct current sensitivity, *Geophys. J. Int.*, **144**, 289–299.
- Tauber, S., Banks, R., Ritter, O., and Weckmann, U., 2003. A high-resolution survey of the Iapetus Suture Zone in south-west Scotland, *Geophys. J. Int.*, **153**, 548–568.
- Thomson, A.W.P., McKay, A.J., Clarke, E. and Reay, S., 2005. Surface electric fields and geomagnetically induced currents in the Scottish Power grid during the 30 October 2003 geomagnetic storm, *Space Weather*, **3**, doi:10.1029/2005SW000156.
- Viljanen, A., 1997. The relation between geomagnetic variations and their time derivatives and implications for estimation of induction risks, *Geophys. Res. Lett.*, **24**, 631–634.
- Viljanen, A., Amm, O. and Pirjola, R., 1999. Modelling geomagnetically induced currents during different ionospheric situations, *J. geophys. Res.*, **104:A12**, 28,059–28,071.
- Viljanen, A. and Pirjola, R., 1994a. Geomagnetically induced currents in the Finnish high-voltage power system: a geophysical review, *Surv. Geophys.*, **15**, 383–408.
- Viljanen, A. and Pirjola, R., 1994b. On the possibility of performing studies of the geoelectric field and ionospheric currents using induction in power systems, *J. Atmos. Sol. Terr. Phys.*, **56**, 1483–1491.
- Weaver, J., 1994. *Mathematical Methods for Geo–electromagnetic Induction*, Research Studies Press Ltd.
- Weaver, J.T., Agarwal, A.K. and Lilley, F.E.M., 2000. Characterization of the magnetotelluric tensor in terms of its invariants, *Geophys. J. Int.*, **141**, 321–336.

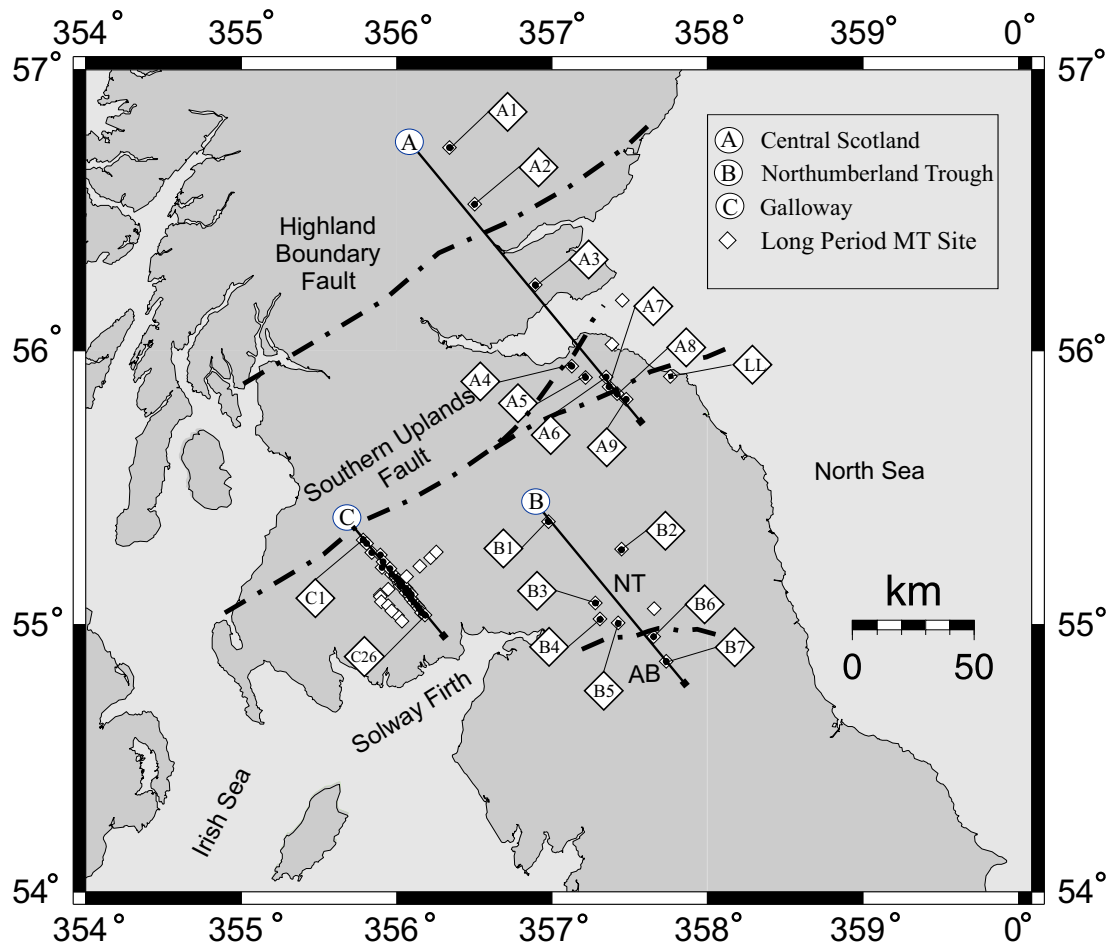


**Figure 1.** The northern England and southern Scotland region showing the available long period (750 s) ‘Iapetus’ Magnetotelluric dataset. Also shown are three profiles A - Central Scotland; B - Northumberland Trough (NT); C - Galloway. AB is the Alston block; bold dot and dash lines indicate major faults.

## FIGURES

This paper has been produced using the Blackwell Publishing GJI L<sup>A</sup>T<sub>E</sub>X2e class file.

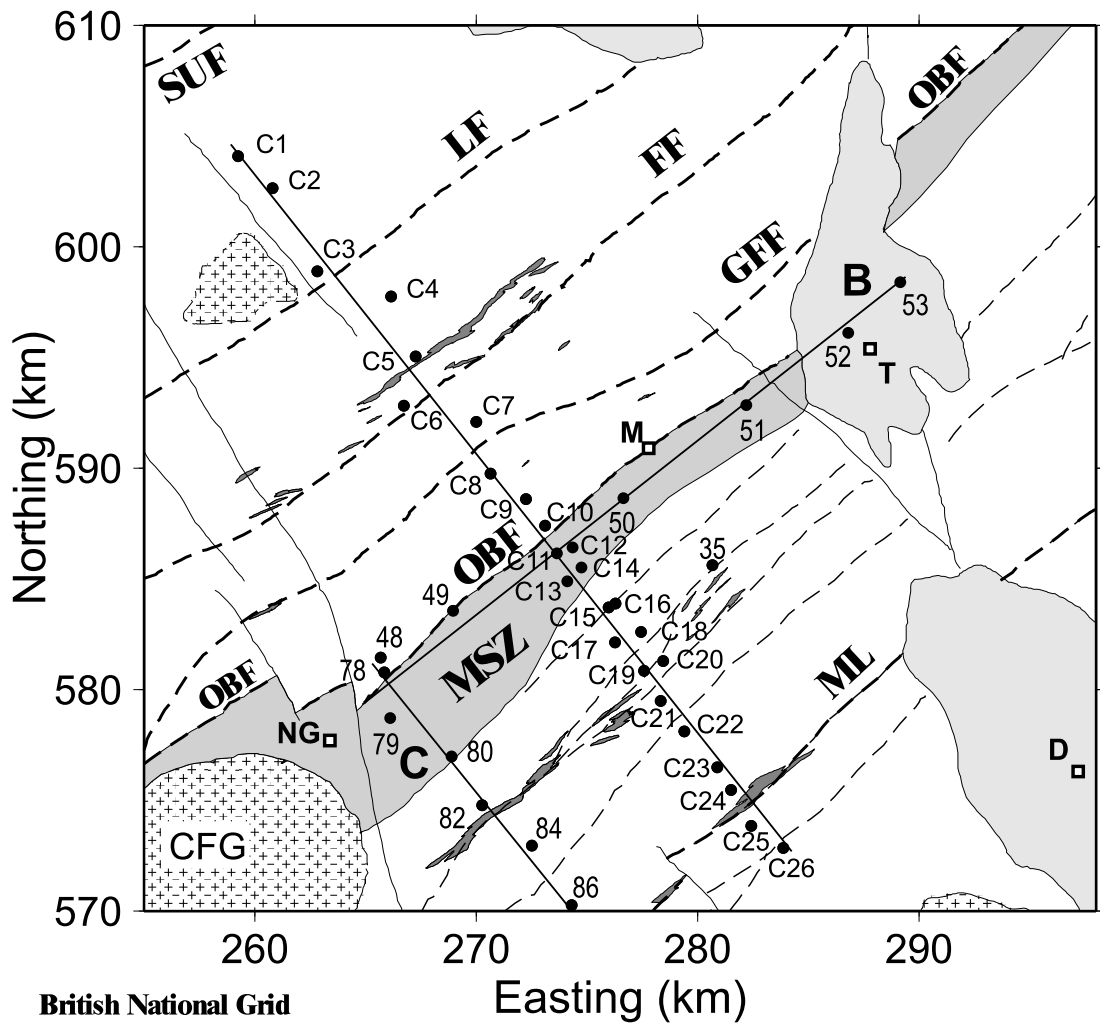


**Figure 2.** Location of MT sites along profile C of Figure 1 in relation to the geology of Galloway. Black dashed lines, NE-SW tract bounding faults (Caledonian); continuous lines, NW-SE normal faults (Carboniferous); unshaded areas, Ordovician and Silurian greywackes; light-shaded areas, Carboniferous/Permian-Triassic sediments; thin dark streaks, carbonaceous shales; broad dark zone, Moniaive Shear Zone (MSZ); ++, granite batholiths (CFG; Cairnsmore of Fleet). SUF; Southern Uplands Fault; LF, Leadhills Fault; FF, Fardingmullach Fault; GFF, Glen Foumart Fault; OBF, Orlock Bridge Fault; ML, Moffat Line. D, Dumfries; T, Thornhill; M, Moniaive; NG, New Galloway. After Tauber et al. (2003).

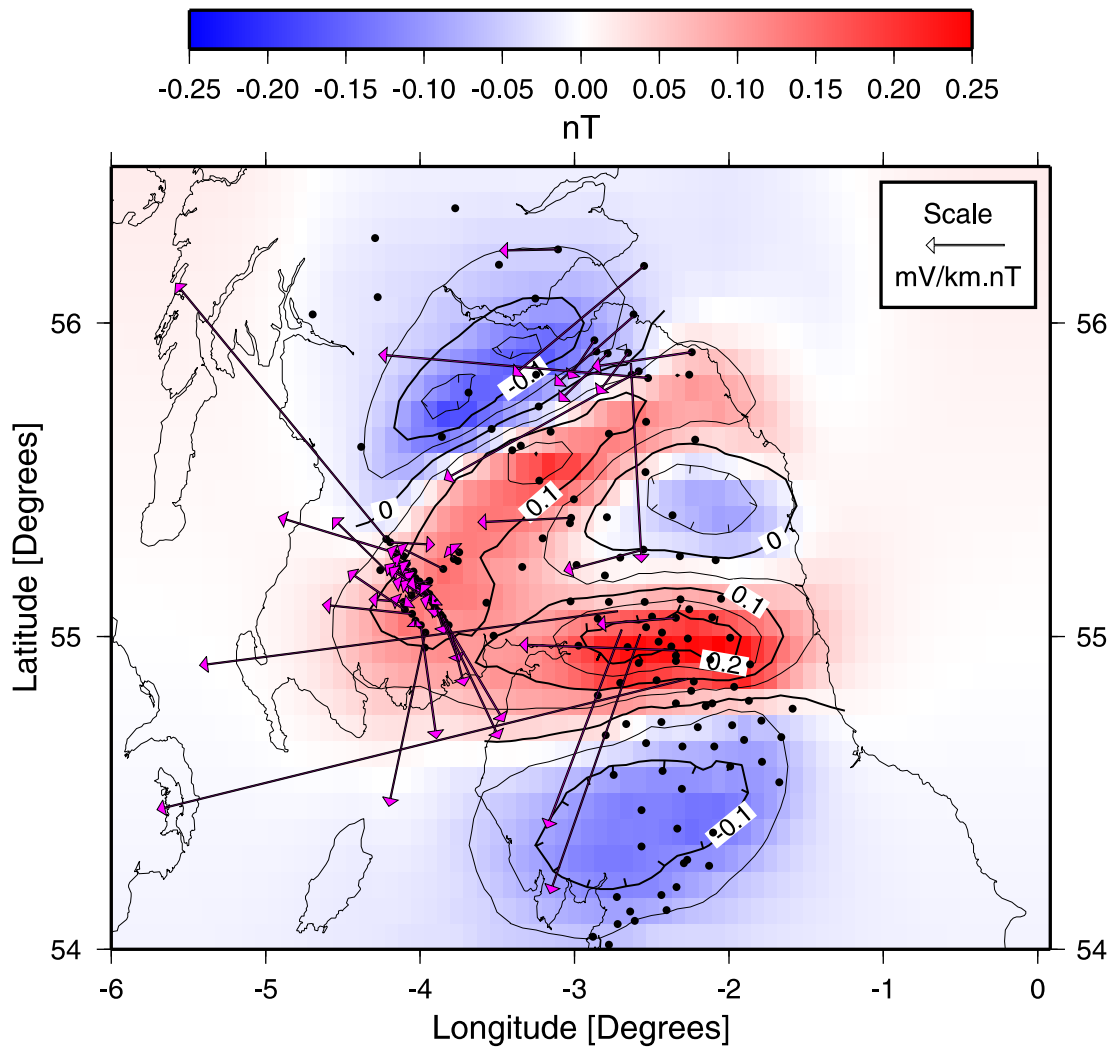


**Figure 3.** Hypothetical event map showing the magnetic variation anomalies (contours and shading) and telluric vectors (arrows) at selected sites in the NESS region. The black dots indicate Geomagnetic Deep Sounding sites.

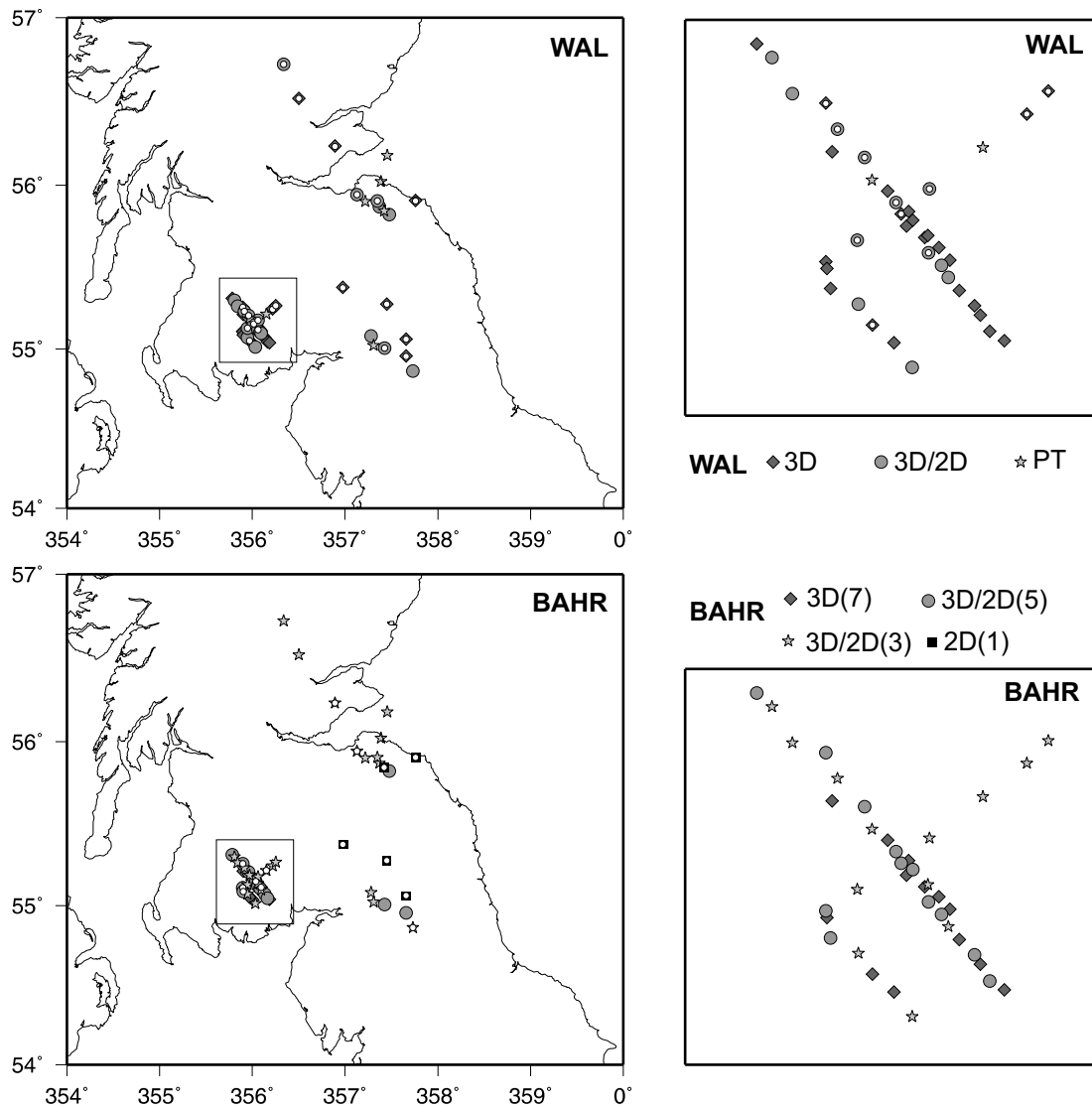


**Figure 4.** Dimensionality of the MT sites using the WAL (top) and Bahr (bottom) criteria. Diamonds - 3D structure; Circles - 3D Galvanic Distortion of a 2D region/ Bahr Class 5; Stars - Pure Twist of the Electric Field (WAL)/ Weak galvanic distortion, Bahr class 3; Squares - 2D region. The white circles highlight sites where the dimensionality was difficult to determine. The Galloway survey of Tauber et al. (2003) has been expanded for clarity. See text for details.

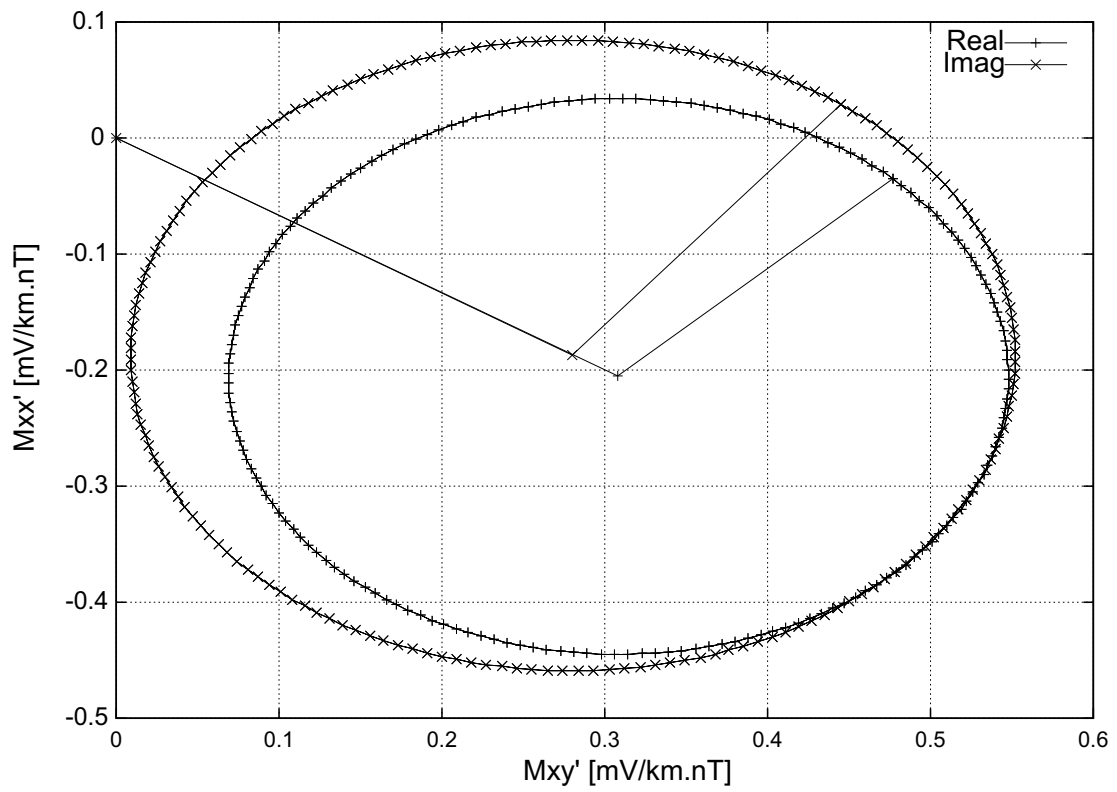


**Figure 5.** Real (+) and Imaginary (x) Mohr circles for the Galloway site C11.

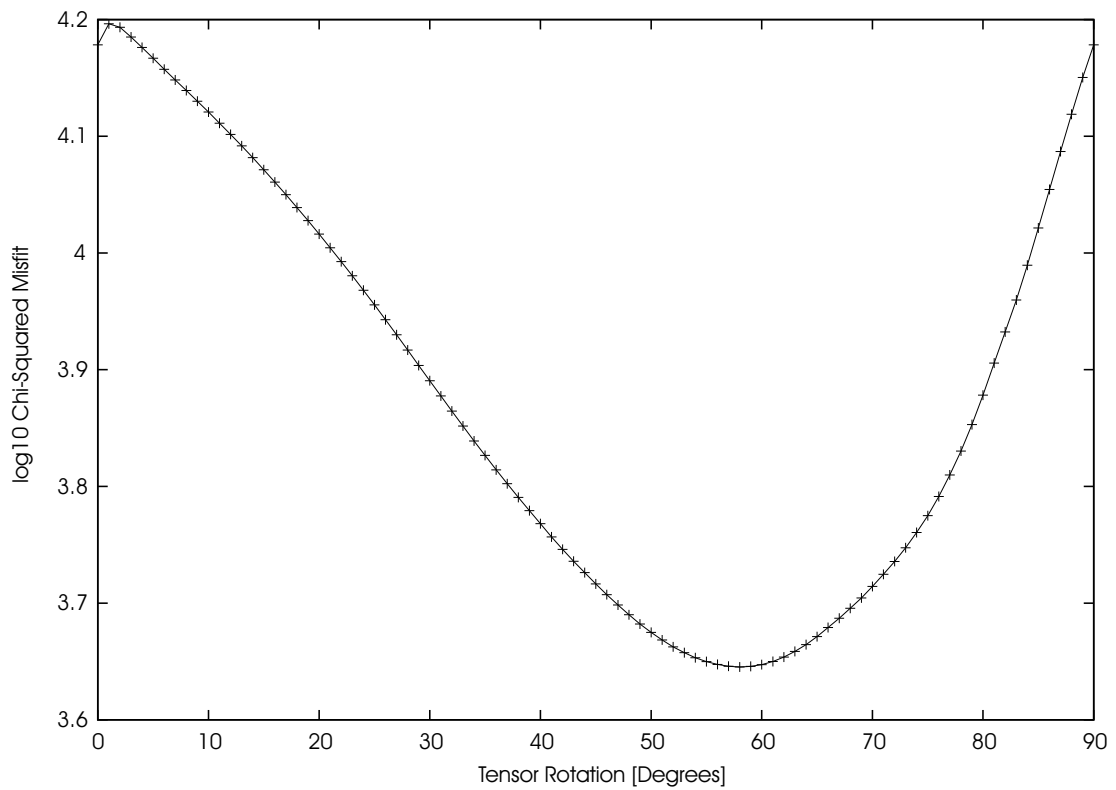


**Figure 6.** Dependence of the total misfit on the angle ( $^{\circ}$ ; clockwise from geographic north) through which the MT tensors of all sites were rotated.

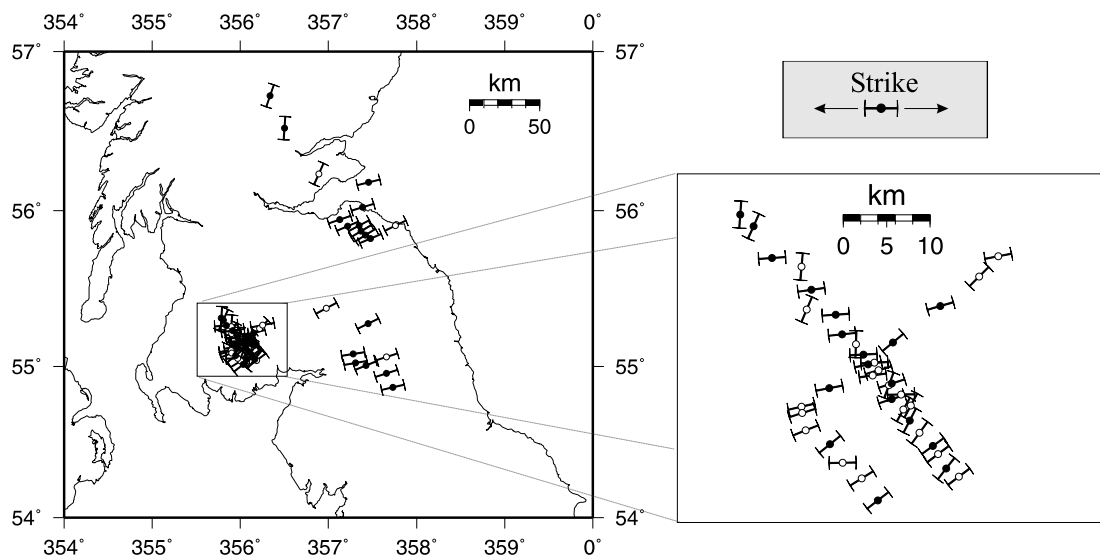


**Figure 7.** Electromagnetic strike (parallel to the side-bars) of each site determined using the method of Smith (1995). Sites which generated an acceptable misfit are shown with filled circles; the unfilled circles denote sites where the fit is poor.

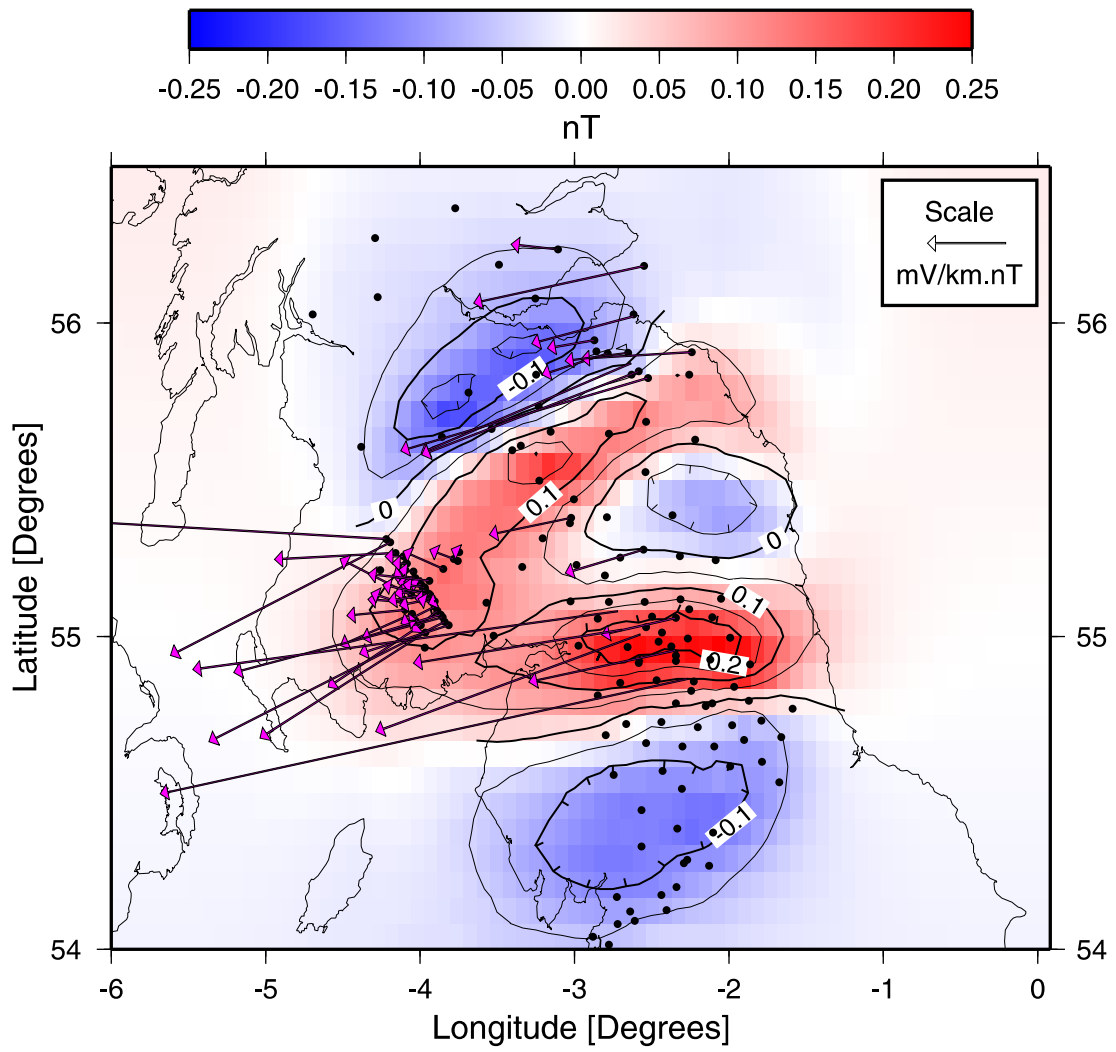


**Figure 8.** The  $e_x$  telluric vectors recovered via tensor decomposition.

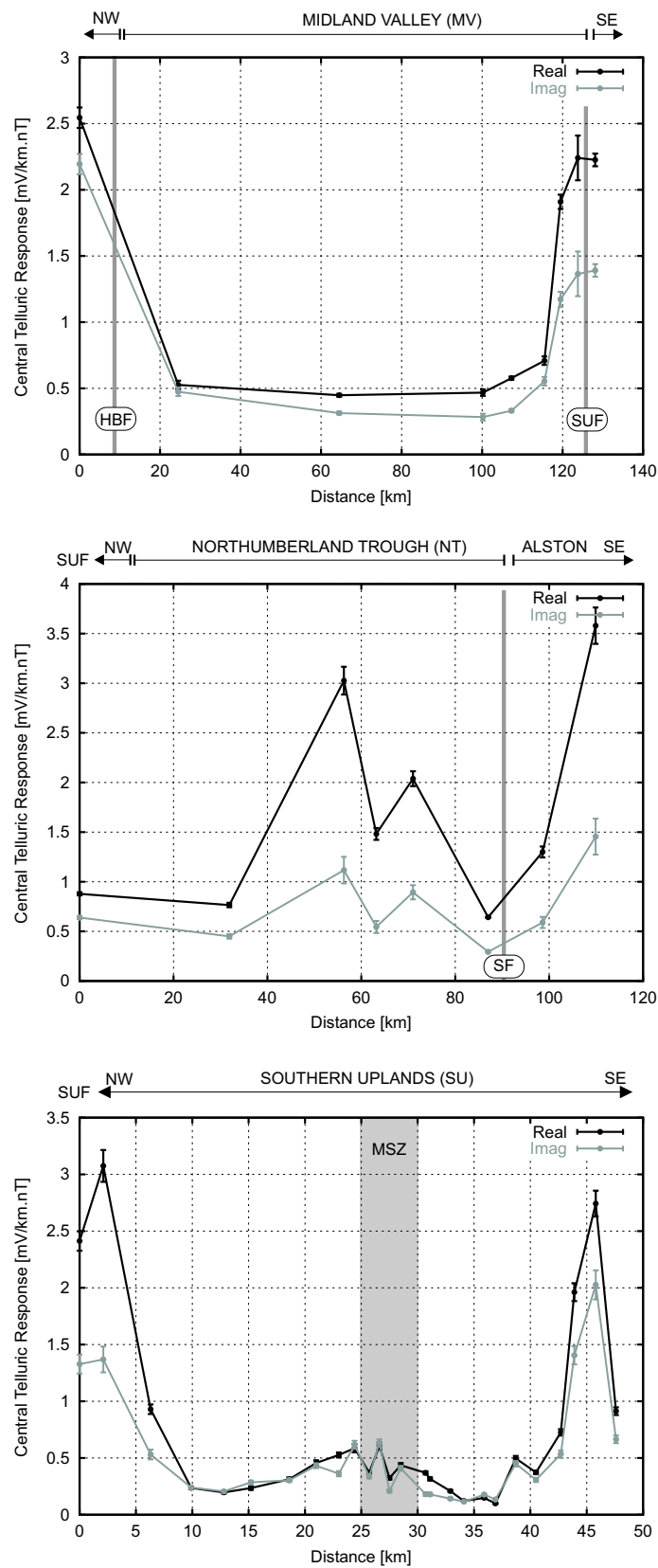


**Figure 9.** The central telluric response for the three NESS profiles. Profile A (top) - Central Scotland; Profile B (middle) - Northumberland Trough; Profile C (bottom) - Galloway. See also Figure 1 and text for further details.